Energy Engineering

Tech Science Press

http://doi.org/10.32604/ee.2026.076359

ARTICLE

# Research on Modeling Single-Phase Tree Contact Faults in Distribution Networks Based on Tree Temperature

**Zhengzheng Fu*, Songhai Fan and Qianqiu Shao**

State Grid Sichuan Electric Power Company Electric Power Science Research Institute, Chengdu, China
*Corresponding Author: Zhengzheng Fu. Email: cathygold@foxmail.com

Received: 19 November 2025; Accepted: 24 July 2026; Published: 12 November 2026

**ABSTRACT:** Tree-contact single-phase-to-ground faults (TSF) along transmission and distribution line corridors can ignite trees, trigger fires, and threaten normal line operation. Existing research remains unclear on the mechanism by which tree temperature influences fault evolution. This study therefore investigates fault current characteristics during TSF. First, numerical relationships between fault currents under tree temperature conditions were derived based on conductive medium transmission mechanisms and equivalent circuit models. Second, a fitting model for tree conductivity versus tree temperature was constructed; these numerical relationships were applied to iterative calculations within the fault model. A tree-line fault model based on tree temperature was established and integrated into the fault model for iterative solution, capturing the dynamic changes in the actual tree state. This enabled simulation of fault currents during the TSF process. Finally, experimental data validated the model, demonstrating that the developed equivalent model accurately fits both the magnitude and waveform of TSF currents. These findings hold significant implications for the detection, diagnosis, and prediction of TSF.

**KEYWORDS:** Conductor-to-tree single-phase ground fault; tree temperature; fault current; fault model

## 1 Introduction

The distribution network is a crucial link of the power system towards the user side, covering a wide area and featuring complex load types. Its operational safety directly affects the power supply quality and public safety. In actual operation, the types of distribution network faults are diverse, among which single-phase high-impedance grounding faults (HIF) occur frequently. Existing statistics and engineering studies have shown that tree-contact faults (TSF) account for a considerable proportion in HIF events [1–4]. However, TSF often exhibits characteristics such as a smaller fault current amplitude and unstable waveform, making it difficult to meet the action threshold of conventional protection devices [5,6]. As a result, the number of high-quality and reproducible TSF fault samples that can be obtained in the field is relatively limited, which in turn restricts the mechanism analysis and model verification [7]. Although TSF faults involve small grounding currents and pose minimal threat to the stability of power equipment and systems, their prolonged persistence carries a high risk of triggering wildfires, severely endangering the lives and property of residents. For instance, the November 2018 California wildfires caused economic losses exceeding $10 billion [8]. In March 2020, a forest fire in Liangshan, Sichuan Province burned 3047 hectares, resulting in direct economic losses of 97.31 million yuan and claiming 19 lives. Therefore, enhancing TSF detection capability is an urgent issue facing modern power systems.

Copyright © 2027 The Authors. Published by Tech Science Press. This work is licensed under a Creative Commons Attribution 4.0 International License, which permits unrestricted use, distribution, and reproduction in any medium, provided the original work is properly cited.

Existing research has categorized TSF failures under HIF failures for study, yet specialized modeling addressing the physical mechanisms and parameter evolution of TSF failures remains insufficient. Given the pronounced nonlinear characteristics of HIF failures, the prevailing view attributes the nonlinear source to the arc process. Consequently, numerous models are based on the Mayr or Cassie arc equivalents with subsequent modifications [9–12]. In addition to arc-based models, the literature [13] proposes a modeling approach based on the current density–electric field strength characteristics of solid media. By segmentally fitting the variation curve of medium conductivity with electric field strength, it obtains a nonlinear resistor that simulates the characteristics of HIF. Due to the inadequate explanation of the physical mechanism of TSFs by existing models, the slow-changing characteristics of their transition resistance can only be corrected using empirical parameters [14,15]. However, given the significant variations in the rate of decline of transition resistance across different TSFs, the empirical parameter correction method exhibits poor universality.

Research on the fault characteristics of TSFs and their influencing factors has been conducted both domestically and internationally. Taking Australia's Powerline Forest Fire Safety Program as an example, typical TSF fault types identified include single-phase tree contact to ground, tree bridging of two-phase lines, and broken conductors igniting dead and fallen vegetation. The literature [16] indicates that TSF fault characteristics are influenced by the combined effects of tree size and species, moisture content, and relative motion between the tree and the line. The literature [17] analyzed and identified the developmental stages of TSF faults, elucidated the TSF mechanism, and summarized the electrical parameters and physical field characteristics of TSF faults. The literature [18] further demonstrates that tree moisture content significantly influences TSF fault characteristics and fault current behavior, establishing a predictive model for tree ignition. Regarding arcs at tree-line contact points, the literature [19] concludes through discharge experiments that gap arc temperature progressively increases as the tree-line distance decreases. The literature [20] investigates arc characteristics at tree-line contact locations and proposes corresponding fault detection methods.

Existing research has identified the fundamental characteristics of TSF faults, but has not sufficiently considered factors such as tree temperature. Consequently, the understanding of tree-contact faults remains incomplete. To address these issues, this paper derives the numerical relationship between tree temperature and TSF fault current. It analyzes the impact of tree temperature on single-phase tree-to-ground fault characteristics from the perspectives of fault current and arc discharge behavior. Subsequently, a relationship model between tree temperature and electrical conductivity is established. The study investigates the evolution process of tree-contact ground faults, obtaining the current variation curve during fault occurrence through numerical simulation.

To provide a clear roadmap of this research, the structure and primary contributions of each section are outlined as follows:

Section 2: Analysis of TSF Parameter Evolution Mechanisms. This chapter analyzes the influence of tree temperature on fault current from both macro-current characteristics and micro-charged particle motion. It defines the four distinct physical stages of fault evolution—initial heating, water evaporation, carbonization, and breakdown—and establishes a dynamic temperature rise model considering Joule heating, heat conduction, convection, radiation, and latent heat of evaporation.

Section 3: Construction of the Fractal Tree-Line Contact Model. Utilizing fractal geometry, this chapter simplifies the complex spatial structure of trees into a self-similar dendritic network to address the limitations of traditional static models. By fitting the binary relationship between conductivity, temperature,

and moisture content, a dynamic equivalent resistance formula is derived that accounts for fractal scaling, enabling the real-time coupling of physical state and electrical parameters.

Section 4: Simulation Modeling and Experimental Validation. A single-phase grounding fault simulation platform is constructed in MATLAB/Simulink, integrating the proposed iterative algorithm. By comparing simulated fault current waveforms with experimental data, this chapter validates the model's accuracy in capturing the magnitude and non-linear trends of TSF currents. Furthermore, it provides guidance on the degree of alignment between laboratory conditions and complex field environments, such as the impact of wind and tree species diversity.

Section 5: Conclusion. This chapter summarizes the dominant role of tree temperature in TSF development and underscores the model's value in enhancing fault diagnosis and wildfire prevention. It also evaluates the implications of assuming uniform physical properties across fractal scales and suggests directions for future refinements.

## 2 Analysis of TSF Parameter Variations

### *2.1 Fault Current Characteristics Analysis*

To more accurately describe the variation pattern of fault currents, the effective value of the fault current is calculated as shown in Eq. (1).

$$I_{\text{rms}} = \sqrt{\frac{1}{T_i}\int_0^{T_i} i^2 dt} \tag{1}$$

In the equation: $I_{\text{rms}}$ and $i$ represent the effective value and instantaneous value of the current, respectively; $T_i$ denotes the period of the current.

Select representative tree specimens for testing, measure and determine the effective value curve of fault currents, as shown in Fig. 1. The results indicate that fault currents also exhibit a phased pattern.

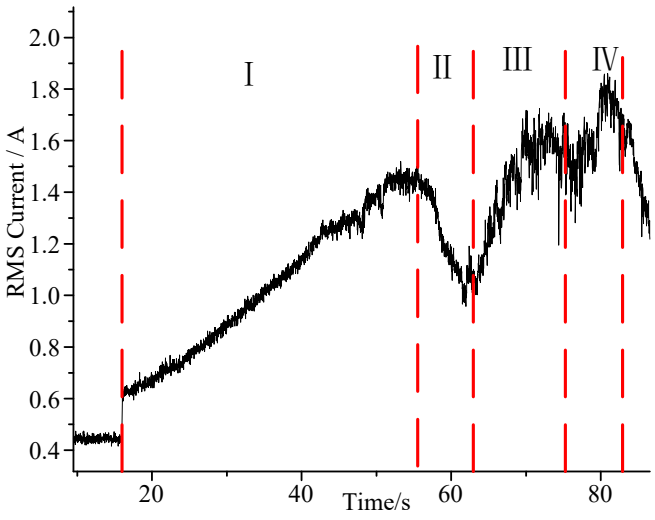



**Figure 1:** RMS curve of fault current flowing through the sample.

Temperature rise can cause increased electrical conductivity in trees, surface charring, and reduced moisture content, leading to changes in the equivalent electrical resistance of trees. The impact of temperature rise on electrical conductivity will be analyzed across four stages.

Stage I: High temperatures at the contact point cause the wood to char and produce visible flames, while electrical Joule heating raises the sample temperature. The electrical conductivity σ of the wood can be expressed as Eq. (2).

$$\log \sigma = D - \frac{0.434 U_0}{2RT\varepsilon} \tag{2}$$

In the equation: $D$ is a constant; $U_0$ is the ionization energy of ions in a vacuum; $R$ is the gas constant; $T$ is the absolute temperature; $\varepsilon$ is the dielectric constant of the material.

From Eq. (2), it can be seen that as temperature rises, $T$ increases, leading to an increase in tree electrical conductivity. Therefore, the fault current in Phase I exhibits a gradually increasing trend.

Stage II: When the temperature reaches 100°C, water inside the tree evaporates and is expelled in large quantities. Based on the relationship between ion concentration and migration rate, the tree's electrical conductivity σ can be expressed as Eq. (3).

$$\sigma = V\mu g F \tag{3}$$

In the equation: $V$ represents the concentration of the electrolyte or salt; $\mu$ denotes the ion mobility; $g$ is the conductivity of the conductive ions; $F$ is the charge factor.

A decrease in moisture content leads to reductions in $\mu$ and $g$, which in turn causes a decline in the tree's electrical conductivity $\sigma$. Consequently, fault currents exhibit a decreasing trend during this phase.

Stage III: When the temperature rises to the charring point of wood (270–450°C), charring pathways form on the tree surface. Since charcoal exhibits high electrical conductivity that increases with temperature, the tree's equivalent impedance decreases. Consequently, fault currents surge dramatically during this stage.

Stage IV: A carbonized channel penetrates the sample's surface layer, while a flame channel traverses the sample surface from one end to the other. Under high-temperature conditions, the resistivity of charcoal decreases sharply [21], causing the equivalent resistance of the tree to drop dramatically. This results in excessive fault current, triggering a circuit breaker trip.

Temperature rise at different stages will exert varying effects on the electrical conductivity of trees, leading to phased changes in current flow. Conversely, by analyzing the fault current variation curve, one can infer the temperature distribution characteristics of trees and the ignition stage, thereby providing a basis for identifying TSF faults.

### *2.2 Mechanism and Computational Model of Tree Temperature Rise*

Based on the thermal effects of electric current and heat transfer principles, the mechanism of temperature rise in trees is analyzed to establish a temperature rise calculation model.

(1) Joule heating from fault currents. Joule heating from fault currents serves as one of the primary heat sources for tree ignition. Analyzing a sufficiently small time interval $\Delta t$, where the equivalent resistance during $\Delta t$ is $R$, the total Joule heat $Q_j$ can be expressed as in Eq. (4).

$$Q_j = I_i^2 R_i \Delta t \tag{4}$$

In the equation: $I_i$ and $R_i$ represent the effective value of the current and the equivalent resistance during the $i$-th cycle, respectively.

(2) Heat conduction in the burning portion. Based on experimental measurements, the average temperature of the burning portion of trees is 500°C. Heat is conducted from the burning portion along the branches

to the unburned portion. Simplified as one-dimensional heat conduction, the heat $Q_T$ conducted from the burning portion during time $\Delta t$ is given by Eq. (5).

$$Q_{\mathrm{T}} = \lambda_v \frac{\Delta T_x}{\Delta x} S \cdot \Delta t \tag{5}$$

In the equation: $\lambda_v$ represents the thermal conductivity coefficient of the object, specifically referring to the thermal conductivity coefficient of typical trees in this paper; $S$ denotes the cross-sectional area of a typical tree; $\Delta T_x$ indicates the temperature difference between the prediction point and the burning section; $\Delta x$ represents the distance between the prediction point and the burning section.

(3) Convective heat transfer. Air flowing over a solid surface carries away part of its heat; this process of heat transfer is called convective heat transfer. The convective heat transfer rate $Q_C$ at the tree surface over time $\Delta t$ can be expressed by Eq. (6).

$$Q_c = h(T_v - T_0)\Delta t \tag{6}$$

In the equation: $h$ is the dimensionless air convective heat transfer coefficient; $T_v$ is the surface temperature of the tree; $T_0$ is the ambient temperature.

(4) Thermal radiation. According to the Stefan-Boltzmann law, the heat $E$ radiated outward by trees per unit time is expressed as Eq. (7).

$$E = \varepsilon_v \delta(T_{\mathrm{vk}}^4 - T_{0\mathrm{k}}^4) \tag{7}$$

In the formula: $\delta$ is the Stefan-Boltzmann constant, $\delta = 5.67 \times 10^{-8}$ W/(m$^2$·K$^4$); $\varepsilon_v$ is the surface emissivity of trees; $T_{\mathrm{vk}}$ is the Kelvin temperature of trees; $T_{0\mathrm{k}}$ is the ambient Kelvin temperature.

(5) Heat dissipation through water evaporation. The evaporation of water within trees consumes heat, with the commonly accepted heat of vaporization parameter $l = 2260$ kJ/kg. The formula for calculating the heat consumed by water evaporation $L$ is shown in Eq. (8). The calculation of the absolute moisture content of the sample [22] is given by Eq. (9).

$$L = \alpha m_W l \tag{8}$$

$$AMC = \frac{M_1 - M_2}{M_2} \times 100\% \tag{9}$$

In the equation: $m_W$ represents the mass of water in the tree, which can be calculated using Eq. (9); $\alpha$ is a coefficient equal to $\alpha = 1$ between 100~120°C, and $\alpha = 0$, otherwise, indicating significant water evaporation at temperatures between 100~120°C.

The specific heat capacity at zero temperature $c_{\mathrm{w0}}$ of a water-containing branch at 25°C can be expressed as Eq. (10).

$$c_{w0} = \frac{c_0 + c_p W}{1 + W} \tag{10}$$

In the equation: $c_0$ and $c_{\mathrm{p}}$ represent the specific heat capacity of absolutely dry wood and saturated water at 25°C, respectively, in kJ/(kg·°C). $W$ denotes the moisture content of the branch.

Considering the effect of temperature, the specific heat capacity of the branch affected by temperature is given by Eq. (11) [3].

$$C_{\mathrm{w}} = C_{\mathrm{w0}} + 1.51 \times 10^{-4}(T_{\mathrm{v}} - T_0) \tag{11}$$

In the formula: $T_v$ and $T_0$ represent the actual temperature and ambient temperature, respectively.

The initial specific heat capacity is determined according to Eq. (10). During the test, as the tree temperature rises, the change in specific heat capacity can be calculated using Eq. (11), thereby continuously updating the specific heat capacity $c_w$.

The equation for the heat of branches per unit time is shown in Eq. (12).

$$Q_J + Q_T - Q_C - E - L = c_w m \Delta T \tag{12}$$

In the equation: $c_w m \Delta T$ represents the heat consumed by the tree during warming; $m$ denotes the mass at the location to be determined; $\Delta T$ signifies the temperature change. Except for L, which is the average value, $Q_J$, $Q_T$, $Q_C$ and E are all functions of temperature.

### *2.3 Mechanism of Tree Media Influence on Fault Current Taking*

Taking Stage I as an example, analyze the mechanism by which the tree medium influences fault current. Conductivity within the tree medium primarily occurs through the movement of free electrons and ions. When voltage U is applied, disregarding the influence of contact resistance on electric field strength, a uniform strong electric field forms within the tree.

Considering the mutual binding effects between charged particles, a comprehensive resistance force $F_s$ is introduced and analyzed at a fixed value. The force analysis for a single charged particle is shown in Fig. 2.

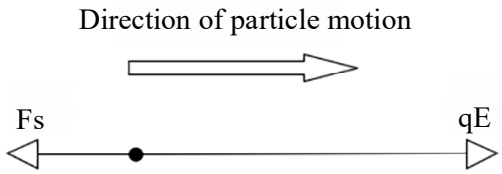



**Figure 2:** Force analysis on charged particles.

Charged particles begin moving from the tree line contact point, pass through the tree trunk, and flow into the ground. During this process, the charged particles gain energy $\Delta Q$, as described by the formula in Eq. (13).

$$\Delta Q = qU - F_s L \tag{13}$$

According to the theorem of conservation of kinetic energy, the velocity $v$ of a charged particle with initial velocity $v_0$ can be expressed as in Eq. (14).

$$v = \sqrt{\frac{2(qU - F_s L)}{m} + v_0^2} \tag{14}$$

The microscopic expression for the particle current is given by Eq. (15).

$$I = nqSv \tag{15}$$

In the formula: $n$ represents the number of particles per unit volume; $S$ denotes the cross-sectional area.

Substituting Eq. (14) into Eq. (15) yields the relationship between current $I$ and the tree's insertion length $L$ and radius $r_0$, expressed as shown in Eq. (16).

$$I{=}nqSv = nq\pi(r_0)^2\sqrt{\frac{2(qU - F_sL)}{m} + v_0^2} \tag{16}$$

From Eq. (16), it can be seen that the current $I$ is negatively correlated with the length $L$. From a microscopic perspective, the tree contact length affects the work done by the internal combined resistance $F_s$ of the conductor, and this effect is positively correlated with the radius $r_0$.

Further analysis of the influence of the medium on fault current from the perspective of current density. Current density is defined as the ratio of the magnitude of current passing through a cross-sectional area to that cross-sectional area, expressed as shown in Eq. (17).

$$J = \frac{I}{S} \tag{17}$$

In the equation: $\mathcal{J}$ represents current density, A/cm$^2$; $I$ represents current magnitude, A.

Current density is determined by the effective value of the current and the cross-sectional area of the tree. First, analyze the effect of connection length on the volume current density. The formula for calculating conductor resistance is shown in Eq. (18).

$$R = \rho\frac{L}{S} \tag{18}$$

Substituting Ohm's law into Eq. (18) yields Eq. (19).

$$I = \frac{US}{\rho L} \tag{19}$$

Substituting Eq. (19) into Eq. (17) yields Eq. (20).

$$J = \frac{U}{\rho L} \tag{20}$$

Based on experimental data, the relationship between current density $\mathcal{J}$ and tree length $L$ was fitted as shown in Eq. (21).

$$J = \frac{0.1049}{L + 0.8924} \tag{21}$$

## 3 Tree Contact Line Model

Trees are approximated as cylinders with uniform electrical and thermal properties, ignoring transitional sections between branches, to simplify the model structure for computational convenience. The electrical conductivity of trees is influenced by temperature, making tree temperature a key parameter in the model. By modeling the electrical and thermal properties of trees, the model achieves accurate simulation of TSF currents and their development processes.

Trees, as quintessential natural fractal structures, exhibit similar geometric characteristics across all levels—from the trunk to branches and down to the smallest twigs—in their overall morphology. The fractal tree network model simplifies the simulation of real tree morphology, as shown in Fig. 3. The structural

dimensions decrease proportionally between adjacent levels. Since the TSF pathway consists of only one root and trunk per level, the specific number of branches is not discussed. The tree-like branching network possesses an infinite number of branching layers.

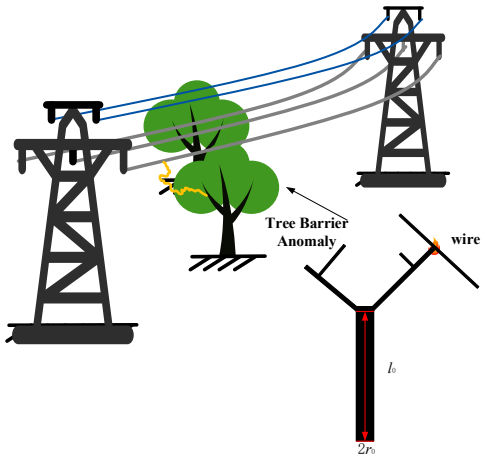



**Figure 3:** Fractal dendritic network model diagram.

In the tree model, $\alpha$ and $\beta$ are defined as the branch length ratio and radius ratio of the $k$ + 1th layer network branch and the $k$th layer network branch, respectively, as follows:

$$\begin{cases} \alpha = \frac{l_{k+1}}{l_k} \\ \beta = \frac{r_{k+1}}{r_k} \end{cases} \tag{22}$$

In the formula, $l_k$ and $l_{k+1}$ represent the branch lengths of the $k$th-layer network and the $k$ + 1th-layer network, respectively, while $r_k$ and $r_{k+1}$ denote the branch radii of the $k$th-layer network and the $k$ + 1th-layer network, respectively.

For $l_k$ and $r_k$, we have:

$$\begin{cases} l_k = l_0 \alpha^k \\ r_k = r_0 \alpha^k \end{cases} \tag{23}$$

In the equation, $l_0$ represents the base branch length in the tree model, the trunk height, and $r_0$ denotes the base branch radius, the trunk radius.

After aligning the updated tree temperature and transition resistance data over time, a least-squares method was used to fit the data, yielding the relationship between tree model conductivity and temperature. The fitted relationship between conductivity and temperature is expressed as follows:

$$\ln\sigma_t(W, T) = 7.458W + 0.057T - 0.050W \times T - 10.754 \tag{24}$$

In the equation, $\sigma_t(W, T)$ represents the conductivity calculated at time $t$ relative to temperature and moisture content, where $W$ denotes tree moisture content and $T$ denotes tree temperature.

Applying the aforementioned binary relationship to the single-phase tree fault model, iterative calculations are performed to obtain the tree temperature rise. Based on this temperature rise, the tree's temperature is recorded throughout the entire process. The iterative calculations are grounded in the

relationship between tree path resistance and moisture content/temperature. In the single-phase tree fault model, the tree path resistance $R_t$ is calculated as follows:

$$R_t = \sum_{k=1}^{n} \left( \frac{\alpha}{\beta^2} \right)^k \frac{l_0}{\pi \sigma_t(W, T) r_0^2} \tag{25}$$

In the equation, $\alpha$ and $\beta$ represent the branch length ratio and radius ratio of the $k$ + 1th layer network branch and the $k$th layer network branch, respectively. $n$ denotes the layer of the contact line in the tree model. $l_0$ is the base branch length in the tree model, the trunk height. $r_0$ is the base branch radius, the trunk radius. $\sigma_t(W, T)$ relationship between tree model conductivity and temperature.

## 4 Single-Phase TSF Model Simulation Verification

### *4.1 Simulation Platform Establishment and Results Analysis*

Tree-line ground faults represent typical high-resistance ground faults. The high ground resistance introduced by trees results in an extremely short fault transient process, allowing the system to rapidly reach steady state. Therefore, this paper neglects the transient process and focuses on analyzing the steady-state fault condition. Taking an ungrounded neutral system as an example, the healthy line can be simplified using lumped parameters. Thus, the external circuit of the simulation model can be represented by an equivalent circuit considering only the line-to-ground capacitance, as shown in Fig. 4 and Table 1. This paper implements the calculation of fault resistance $R_f$ using MATLAB software and simulates tree-contact faults through Simulink. The specific parameters in this simulation structure are as follows: The lengths of the overhead lines are $l_1$ = 3 km, $l_2$ = 6 km, and $l_3$ = 9 km. The overhead line parameters are shown in the table below.

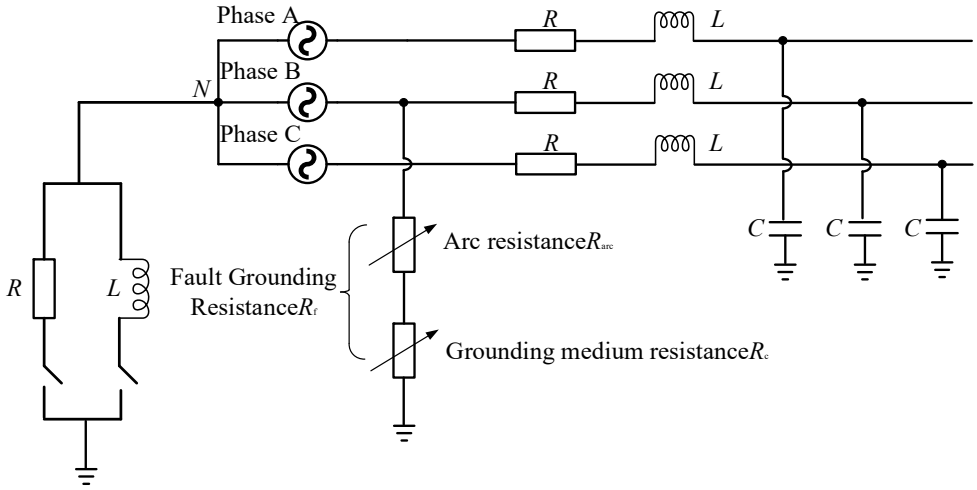



**Figure 4:** Centralized parameter equivalent ground fault model for distribution networks.

**Table 1:** Overhead line parameters.

| Overhead Line Parameters | | | |
|---|---|---|---|
| Forward parameters | $R_1$ = 0.45 km | $L_1 = 1.21 \times 10^{-3}$ H/km | $C_1 = 0.0397 \times 10^{-6}$ F/km |
| Zero-sequence parameters | $R_0$ = 0.7 km | $L_0 = 5.47 \times 10^{-3}$ H/km | $C_0 = 0.0213 \times 10^{-6}$ F/km |

### *4.2 Waveform Simulation Results*

Based on the tree-line arc grounding fault model established in this paper and following the fault modeling process shown in Fig. 4, simulations were conducted under different conditions for verification. Firstly, the specific parameters of Branch 1 and Branch 2 were input into the model, and the comparison curves of the measured and simulated fault phase currents are shown in Figs. 5 and 6. Subsequently, by adjusting the system parameters, the operating states with system capacitive currents of 4.3 A and 8.7 A were simulated, and the results are presented in Figs. 7 and 8. Finally, by changing the tree parameters, simulations were carried out for scenarios with diameters (or sizes) of 4 cm and 6 cm, and the results are shown in Figs. 9 and 10. Statistical results indicate that the correlation coefficients between the simulated and measured waveforms under the above different conditions are 0.9885, 0.9773, 0.9931, 0.9835, 0.9975, and 0.9887, respectively. The data demonstrate that the simulated waveforms of the fault phase current are highly consistent with the measured trends, with high fitting accuracy, effectively verifying the accuracy and universality of the established equivalent model.

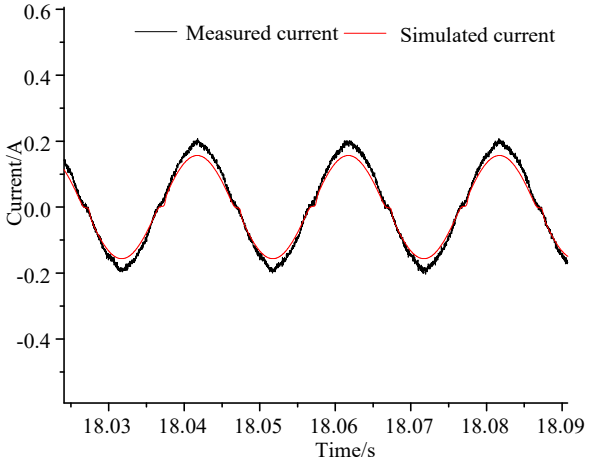



**Figure 5:** Branch 1 model simulation waveform.

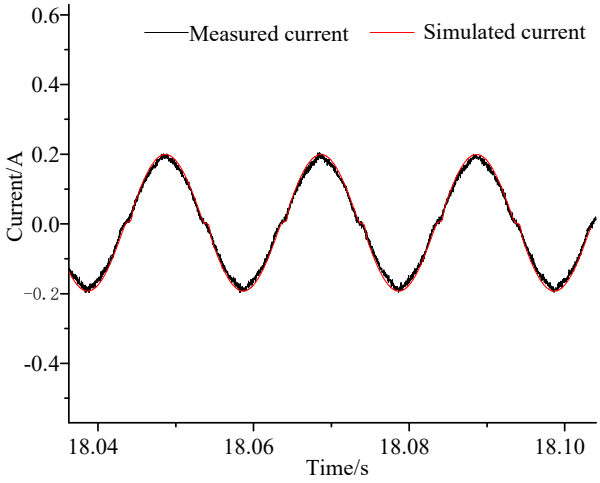



**Figure 6:** Branch 2 model simulation waveform.

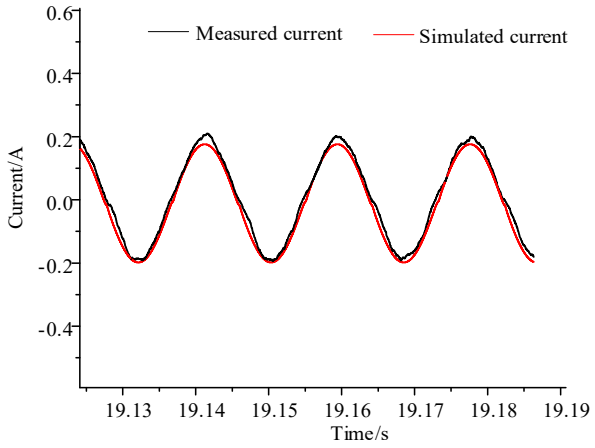



**Figure 7:** Capacitive current is 4.3 A and the simulation waveform is shown.

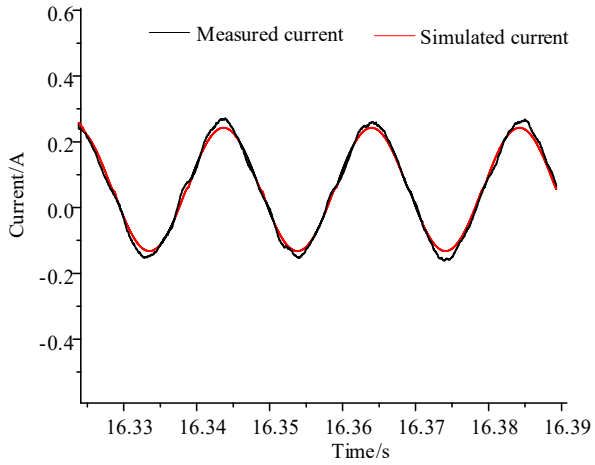



**Figure 8:** Capacitive current is 8.7 A and the simulation waveform is shown.

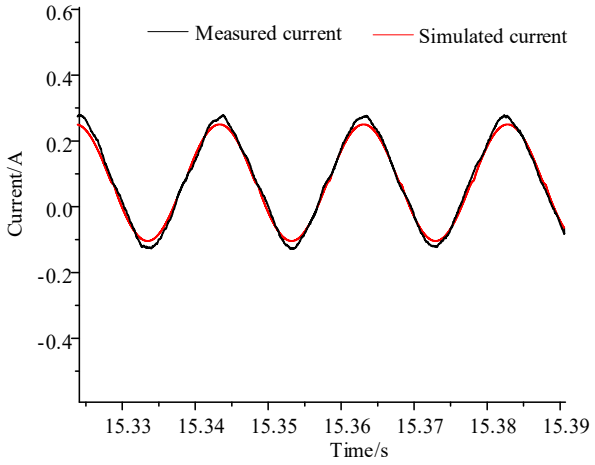



**Figure 9:** The size of the tree is 4 cm in simulated waveform.

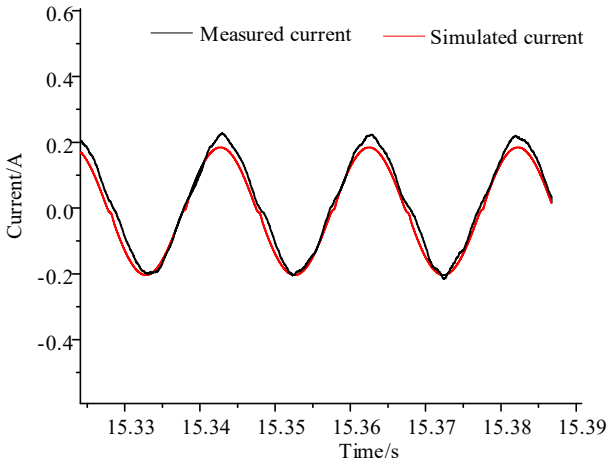



**Figure 10:** The size of the tree is 6 cm in simulated waveform.

## 5 Conclusion

This paper analyzes the physical process during the tree contact fault, utilizes the relationship between tree resistivity and temperature to construct an equivalent circuit model for tree contact faults in a neutral point ungrounded system, studies the influence of tree temperature on the TSF process, derives the mechanism of the role of tree temperature in the development of TSF, investigates the influence law of tree temperature on the fault current, and formulates the fault model considering tree temperature. Based on the tree-line fault model considering tree temperature, it is embedded into the fault model for iterative solution to depict the dynamic changes of the real state of the tree. A model was built in the Simulink simulation software, and the simulation waveforms of the fault current showed the same trend as the measured waveforms, the simulation was relatively accurate, and it could clearly demonstrate the fault characteristics of TSF, providing a new approach for the modeling and simulation of TSF.

**Acknowledgement:** Not applicable.

**Funding Statement:** This research was funded by the State Grid Sichuan Electric Power Company Employee Technological Innovation Project, Research on Grounding Fault Characteristics and Fault Location of 35 kV Transmission Lines Taking into Account Vegetation Burning Characteristics, Grant Number B7199725001W.

**Author Contributions:** Theoretical analysis, experimental operation and writing original manuscript, Zhengzheng Fu; experimental operation, Songhai Fan; data analysis and visualization, Qianqiu Shao. All authors reviewed and approved the final version of the manuscript.

**Availability of Data and Materials:** Data is contained within the article.

**Ethics Approval:** This study did not involve human participants or experimental animals. Therefore, ethical approval was not applicable.

**Conflicts of Interest:** The authors declare no conflict of interest.

## References

1. Cong Z, Liu Y, Yan Y, Wang P, Fang J, Wang K, et al. Study on the mechanism and electrical characterization of the tree-contact incipient fault in the non-effectively grounded system. IEEE Trans Power Deliv. 2023;38(3):1709–19. [CrossRef].

2. He J, Zhou Y, Li Y, Zhang G, Liang J, Shang H, et al. Characteristic quantity analysis of single-phase contact tree ground fault of distribution network overhead lines. Energies. 2023;17(1):132. [CrossRef].
3. Jiang C, Bi M, Zhang S, Li K, Lei S, Jiang T. Study on arc characteristics and combustion feature of tree-wire discharge fault in distribution line. Electr Power Syst Res. 2024;230:110210. [CrossRef].
4. Hu J, Meng W, Wang Z, Deng H, Song Z, Zhu T, et al. The E–I characteristic model based on the composition mole ratio of an arc on the ice surface. IEEE Trans Dielect Electr Insul. 2023;30(3):1265–73. [CrossRef].
5. Yang C, Zhang W, Tang R, Xiao X. Tree-related high-impedance fault in distribution systems: modeling, detection, and ignition risk assessment. Energies. 2025;18(3):548. [CrossRef].
6. Liang D, Xu B, Wang P, Wang W. Comprehensive study on tree-contact single-phase-to-ground faults: modelling, risk analysis, and detection recommendations. High Volt. 2024;9(6):1280–7. [CrossRef].
7. Qin X, Wang P, Liu Y, Guo L, Sheng G, Jiang X. Research on distribution network fault recognition method based on time-frequency characteristics of fault waveforms. IEEE Access. 2018;6:7291–300. [CrossRef].
8. Keeley JE, Syphard AD. Large California wildfires: 2020 fires in historical context. Fire Ecol. 2021;17(1):22. [CrossRef].
9. Ghaderi A, Ali Mohammadpour H, Ginn HL, Shin YJ. High-impedance fault detection in the distribution network using the time-frequency-based algorithm. IEEE Trans Power Deliv. 2015;30(3):1260–8. [CrossRef].
10. dos Santos WC, de Souza BA, Brito NSD, Costa FB, Paes MRC Jr. High impedance faults: from field tests to modeling. J Control Autom Electr Syst. 2013;24(6):885–96. [CrossRef].
11. Bhandia R, de Jesus Chavez J, Cvetković M, Palensky P. High impedance fault detection using advanced distortion detection technique. IEEE Trans Power Deliv. 2020;35(6):2598–611. [CrossRef].
12. Wang B, Liang CG, Li FT. Arc modeling and single-end fault location for arc grounding fault in transmission line considering arc gap length. Proc CSEE. 2019;39(4):1001–9. (In Chinese).
13. Novak T. The effects of very-high-resistance grounding on the selectivity of ground-fault relaying in high-voltage longwall power systems. IEEE Trans Ind Appl. 2001;37(2):398–406. [CrossRef].
14. Wei M, Liu W, Shi F, Zhang H, Jin Z, Chen W. Distortion-controllable arc modeling for high impedance arc fault in the distribution network. IEEE Trans Power Deliv. 2021;36(1):52–63. [CrossRef].
15. Dong CY, He JH, Wang XK, Xu JF, Yu L, Bo ZQ. High-resistance grounding fault detection and location in DC railway system. In: Proceedings of the 11th IET International Conference on Developments in Power Systems Protection (DPSP 2012); 2012 Apr 23–26; Birmingham, UK. [CrossRef].
16. Miller C, Plucinski M, Sullivan A, Stephenson A, Huston C, Charman K, et al. Electrically caused wildfires in Victoria, Australia are over-represented when fire danger is elevated. Landsc Urban Plan. 2017;167:267–74. [CrossRef].
17. Zhou T, Yuan T, Yang Q, Liu H. Arc grounding fault model based on the dynamic characteristics of the entire process of distribution cherry tree related fault. Electr Power Syst Res. 2025;247:111781. [CrossRef].
18. Jiang C, Fan B, Yu K, Wang Z, Zeng X, Wang W. Multiphysical field simulation and experimental verification of initial stage of tree-contact arc grounding fault in distribution networks. IEEE Trans Power Deliv. 2026;41(2):697–710. [CrossRef].
19. Cong ZH, Liu YD, Yan YJ, Fang J, Jiang XC. Simulation analysis of early tree-to-line faults in distribution lines based on magnetohydrodynamics. Trans China Electrotech Soc. 2020;35(S2):562–8. (In Chinese).
20. Xu J, Wu Q, Zhang X, Zhang G. Improved Mayr-cassie combinatorial arc model of tree contact incipient fault simplified by MHD. In: Proceedings of the 2024 7th International Conference on Electric Power Equipment-Switching Technology (ICEPE-ST); 2024 Nov 10–13; Xiamen, China. [CrossRef].
21. Wang SY, Hung CP. Electromagnetic shielding efficiency of the electric field of charcoal from six wood species. J Wood Sci. 2003;49(5):450–4. [CrossRef].
22. Ning X, Wen J, Zhang H, Wang J, Sun Z. Analysis of the influence of vegetation size on single-phase contact tree grounding fault characteristics. In: Proceedings of the 2023 Panda Forum on Power and Energy (PandaFPE); 2023 Apr 27–30; Chengdu, China. [CrossRef].